Available online at www.sciencedirect.com
SCIENCE DIRECT®
Pergamon
Acta Materialia XX (2003) XXX–XXX
Acta MATERIALIA
www.actamat-journals.com

Atomistic simulations of B1–B2 phase transition in KCl based on inversion pair potentials

Shuo Zhang *, Nanxian Chen

Department of Physics, Tsinghua University, Room 4303, Beijing 100084, China
Institute of Applied Physics, Beijing University of Science and Technology, Beijing 100083, China

Received 28 March 2003; received in revised form 25 July 2003; accepted 26 July 2003

Abstract

Based on the Chen–Möbius lattice inversion, interionic pair potentials are derived from the pseudopotential total energies of KCl in B1, B2, B3 and one tetragonal structures. In terms of inversion potentials, four different transition pathways have been presented to describe the B1–B2 phase transition by using unit cells with different symmetric restrictions and sizes. Although the intermediate states are obviously different along the four pathways, the simulations indicate that the essence of phase transition is reflected by a Buerger mechanism. With more independent variables than the Buerger and WTM mechanisms, the present potentials predict that the transition path is formed by a series of states with different subgroup symmetries between $Fm\bar{3}m$ and $Pm\bar{3}m$. This indicates that fewer symmetry restrictions will introduce intermediate structures with low symmetry along the transition path. One of the predicted intermediate structures is in good agreement with that found in the B1–B2 phase transition of AgCl. The exhibited transition characters also indicate that the present inversion pair potentials are appropriate in exploring the B1–B2 phase transition in KCl crystal.

Keywords: Modelling; Phase transformation; Crystal structure; Ionic compounds

1. Introduction

Since Al'tshuler et al. [1] first reported the polymorphism of potassium chloride under shock compression, its B1 (NaCl-type) to B2 (CsCl-type) pressure-induced phase transition has attracted considerable attention in experimental and theoretical studies [2–6]. The mechanism of B1–B2 phase transition can usually be explained by two typical models [7–14]. The first is often called the Buerger mechanism [7], which uses a two-ion rhombohedral primitive cell ($a = b = c$, $\alpha = \beta = \gamma = 60°$) to take account of phase transition. When the rhombohedral cell is compressed along one of its threefold axes, the angle α increases from 60° to 90° for accomplishing the B1–B2 phase transition. The second model was proposed by Watanabe, Tokonami and Morimoto (WTM) [8] in their study of phase transition in CsCl. They considered that the B1–B2 phase transition was caused by a highly concerted intralayer rearrangement of atoms associated with interlayer transitions.

* Corresponding author. Tel: +86-106-277-2783; fax: +86-106-277-2783.
E-mail address: zhangshuo@mails.tsinghua.edu.cn (S. Zhang).

1359-6454/$30.00 © 2003 Published by Elsevier Ltd on behalf of Acta Materialia Inc.
doi:10.1016/S1359-6454(03)00434-8

Based on the two models, many calculations [9–14] have been performed to understand the mechanism of B1–B2 phase transition. According to the empirical interionic pair potentials model, the WTM mechanism was considered to be the most reasonable in Nakagiri [9] and Ruff's studies [10]. With similar interionic potentials, Nga and Ong [11] used different constant-pressure molecular dynamics algorithms to explain the equivalence between the Buerger and WTM mechanisms. Similar results were also obtained by Sims [13,14] using both two-body potentials and first-principle periodic Hatree–Fock theory. Their calculations and Pendás's previous work [12] all suggested that the symmetry of the unit cell played an important role in simulations of B1–B2 phase transition. To some extent, the symmetry of the unit cell is the key to simplifying the problems for searching for the transition path on the energy hypersurface. With the constrain of symmetry *R*3*m* (no. 166), the Buerger mechanism takes the (a, a, a, α, α, α) rhombohedral cell as the intermediate states from B1 to B2, and the *Pmm*2 (25) transition path has been determined on the four-dimensional energy hypersurface by WTM mechanisms. However, both of them searched for the intermediate phases with symmetric restrictions.

In our opinion, the transition path should be the global minimum-energy trace on the high-dimensional energy hypersurface, with fewer restrictions of symmetry and unit cell size. The aim of this work is to determine such a transition path by using the appropriate interionic pair potentials. In order to describe the transition path from B1 to B2 phase, the interionic potentials should reflect not only the properties of the B1 and B2 phases, but also the properties of intermediate states. So the interionic potentials should cover wide ranges of interionic separations and bond angles. However, previous potential calculations [9–14] almost all adopted empirical potentials, which only correctly reproduced the properties around equilibrium B1 state. This may result in the loss of some intermediate structures. We then realized that new kinds of interionic potentials could be introduced to understand the mechanism of B1–B2 phase transition. The new potentials include not only the contributions from B1- and B2-KCl crystals, but also those from other phases so as to cover more phase space. Therefore, in addition to the B1 and B2 structures, B3 and T1 (a tetragonal structure with space group *P*4/*mmm* (1 2 3)) models are involved, as shown in Fig. 1. Their lattice constants are from a = 4.5 to 10.0 Å, and even extend to 16.0 Å for B1- and B3-KCl. The total energies of KCl crystals in these four structures are calculated by the pseudopotential method. This leads to the construction of a special phase space, including the equilibrium and non-equilibrium states of B1, B2, B4 and T1 phases. Based on Chen–Möbius lattice inversion [15,16], the interionic pair potentials are extracted from this phase space without any prior potential function forms. Suitable potential function forms are chosen in terms of the resulting potential curves.

With the inversion pair potentials, four minimum-energy transition pathways have been presented in two-ion rhombohedral and eight-ion standard cells within different symmetric limits. Their activation energy barriers and structural variations along the transition path are presented to indicate the influence of cell size and symmetric restrictions. The details are described in the following text.

2. Derivation of interionic pair potentials

As a rock salt-type ionic crystal, the lattice energy of B1-KCl is the sum over all pair potentials. The total energy per KCl pair can be written as

$$E_{\text{total}}^{\text{B1}} = \frac{1}{2}\sum_{i \neq j}\Phi_{++}(r_{ij}) + \frac{1}{2}\sum_{m \neq n}\Phi_{--}(r_{mn}) + \sum_{k \neq l}\Phi_{+-}(r_{kl}) + E_i \quad (1)$$

where r_{ij}, r_{mn} and r_{kl} are separately the cation–cation, anion–anion and cation–anion interionic distances, E_i is the energy of the isolated ions, and Φ_{++}, Φ_{--} and Φ_{+-} are the cation–cation, anion–anion and cation–anion interionic pair potentials, respectively. In order to obtain the above three kinds of pair potentials, the four relative models in Fig. 1 are taken into account simultaneously. The

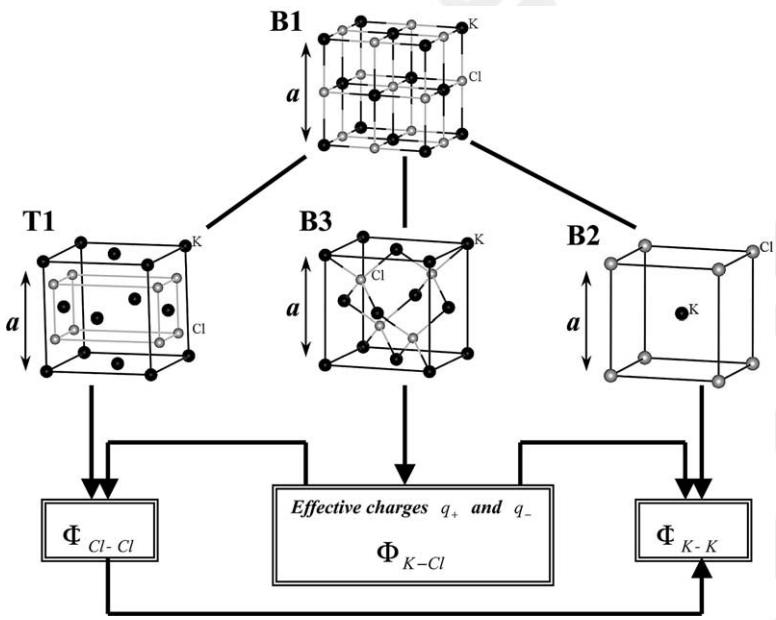

Fig. 1. B1 and its related structures B2, B3 and T1 used for derivation of interionic pair potentials. For every identical lattice constant *a*, the pseudopotential total-energy calculations are performed for the four structures. The scheme shows the derivation of the present interionic pair potentials.

total energies of B1, B2, B3 and T1 KCl crystals are calculated based on the CASTEP (Cambridge Serial Total Energy Package) [17–19], with the pseudopotential plane-wave code developed by MSI [19]. During our ab initio calculations, the ultra-soft pseudopotentials for potassium and chlorine ions are adopted and the GGA-PW method has been used to cope with the exchange-correlation energy. The k-mesh points over the Brillouin zone are generated with parameters $4 \times 4 \times 4$ for the largest reciprocal space and $1 \times 1 \times 1$ for the smallest one by the Monkhorst–Pack scheme [20] corresponding to lattice constant *a*. The energy tolerance for SCF (self-consistent field) convergence is 2×10^{-6} eV/atom, and the kinetic energy cutoff for the plane wave basis set is 260 eV. Fig. 2 shows the calculated total energies of B1, B2, B3 and T1 type KCl crystals as a function of lattice constant *a*.

In our scheme, the Coulombic and short-range potentials are derived separately. The Coulombic part is considered using the fixed effective charges on ions. Since the Coulombic interaction is the long-range part and has slow convergence, the

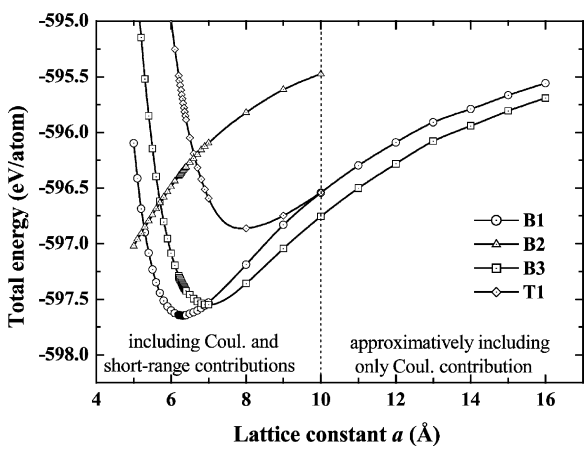

Fig. 2. The pseudopotential total energies as functions of lattice constant *a* in B1, B2, B3 and T1 KCl.

total-energy difference between B1- and B3-KCl can be considered to be only due to Coulombic interaction at a larger lattice constant. With the Madelung constants of B1 and B3 [21], the effective charges q^+ and q^- can be determined by fitting the Madelung energy difference to the total-energy

difference between B1- and B3-KCl when the lattice constant a is larger than 10.0 Å.

As for short-range interaction, it is obvious that both the B1 and B3 structures are formed by two face-centred cubic sublattices of opposite-sign ions. Their difference is just the relative displacement between the cation and anion sublattices. With the same lattice constant a, the total-energy difference per ion between B1- and B3-KCl is only about cation–anion potential Φ_{+-}, which includes the short-range potential $\phi^{SR}_{+-}(r)$ and the Coulomb part $\phi^{Coul}_{+-}(r)$. We then have

$$\Phi_{+-}(r) = \phi^{SR}_{+-}(r) + \phi^{Coul}_{+-}(r) = \phi^{SR}_{+-}(r) + \frac{q_+ q_-}{4\pi\varepsilon_0 r}, \quad (2)$$

with the effective charges q^+ and q^- and total energies $E^{B1}_{total}(a)$ and $E^{B3}_{total}(a)$. The short-range interaction difference between B1- and B3-KCl is

$$\Delta E^{SR}_{+-}(a) = E^{B1}_{total}(a) - E^{B1}_{Coul}(a) - E^{B3}_{total}(a) + E^{B3}_{Coul}(a) = \frac{1}{2}\sum_{i,j,k}\left\{\phi^{SR}_{+-}\left[\sqrt{(i+j-1)^2+(i+k-1)^2+(j+k-1)^2}\frac{a}{2}\right] - \phi^{SR}_{+-}\left[\sqrt{\left(i+j-\frac{1}{2}\right)^2+\left(i+k-\frac{1}{2}\right)^2+\left(j+k-\frac{1}{2}\right)^2}\frac{a}{2}\right]\right\} = \frac{1}{2}\sum_{n=1}^{\infty} R_{+-}(n)\phi^{SR}_{+-}[B_{+-}(n)]x, \quad (x = \sqrt{3}a/4), \quad (3)$$

in which the B1 and B3 Coulomb interactions $E^{B1}_{Coul}(a)$ and $E^{B3}_{Coul}(a)$ can be calculated based on the effective charges and Madelung constants or Ewald summation techniques [22], x is the nearest cation–anion distance in B3 structure, $B_{+-}(n)x$ is the nth-neighbour distance, and $R_{+-}(n)$ is the nth coordination number. According to Chen–Möbius lattice inversion [15,16], $\{B_{+-}(n)\}$ is extended into a multiplicative semi-group $\{b_{+-}(n)\}$ such that, for any two integers m and n, there always exists an integer k such that

$$b_{+-}(k) = b_{+-}(m)b_{+-}(n). \quad (4)$$

Eq. 3 can then be rewritten as

$$\Delta E^{SR}_{+-}(a) = \frac{1}{2}\sum_{n=1}^{\infty} r_{+-}(n)\phi^{SR}_{+-}[b_{+-}(n)x], \quad (5)$$

where

$$r_{+-}(n) = \begin{cases} R(B^{-1}_{+-}[b_{+-}(n)]) & \text{if } b_{+-}(n) \in \{B_{+-}(n)\} \\ 0 & \text{if } b_{+-}(n) \notin \{B_{+-}(n)\} \end{cases}. \quad (6)$$

Thus, the cation–anion short-range pair potential ϕ^{SR}_{+-} can be expressed as

$$\phi^{SR}_{+-}(r) = 2\sum_{n=1}^{\infty} I_{+-}(n)\Delta E^{SR}_{+-}\left[\frac{4}{\sqrt{3}}b_{+-}(n)r\right] \quad (7)$$

in which the inversion coefficient $I_{+-}(n)$ is given by

$$\sum_{b_{+-}(n)/b_{+-}(k)} I_{+-}(n)r\left(b^{-1}_{+-}\left(\frac{b_{+-}(k)}{b_{+-}(n)}\right)\right) = \delta_{k1}. \quad (8)$$

As for the interactions between like-sign ions, with the identical lattice constant a, the cation–cation interaction is unchanged from B1 to T1 structure. Therefore, with the above cation–anion pair potentials, the short-range anion–anion interaction difference per ion between B1 and T1 can be written as

$$\Delta E^{SR}_{--}(a) = E^{B1}_{total}(a) - E^{B1}_{Coul}(a) - E^{B1-SR}_{+-}(a) - E^{T1}_{total}(a) + E^{B3}_{Coul}(a) + E^{T1-SR}_{+-}(a) = \frac{1}{4}\sum_{i,j,k\neq 0}\left\{\phi^{SR}_{--}\left[\sqrt{(i+j)^2+(i+k)^2+(j+k)^2}\frac{a}{2}\right] - \phi^{SR}_{--}\left[\sqrt{i^2+4j^2+k^2}\frac{a}{2}\right]\right\} \quad (9)$$

For B1- and T1-KCl, the short-range cation–anion interactions $E^{B1-SR}_{+-}(a)$ and $E^{T1-SR}_{+-}(a)$ can be calculated via the above $\phi^{SR}_{+-}(r)$. By the same method of lattice inversion [15,16], the anion–anion short-range pair potential $\phi^{SR}_{--}(r)$ can be derived from Eq. (9).

Since the cation–cation, anion–anion and cation–anion interactions all undergo changes from B1 to B2, the only known is the cation–cation pair potential. Their non-Coulomb cation–cation interaction difference is

$$\Delta E^{SR}_{++}(a) = E^{B1}_{total}(a) - E^{B1}_{Coul}(a) - E^{B1-SR}_{+-}(a) - E^{B1-SR}_{--}(a) - [E^{B2}_{total}(a) - E^{B2}_{Coul}(a) - E^{B2-SR}_{+-}(a) - E^{B2-SR}_{--}(a)] = \frac{1}{4}\sum_{i,j,k\neq 0} \quad (10)$$

$$\left\{\phi_{++}^{\mathrm{SR}}\left[\sqrt{(i+j)^2+(i+k)^2+(j+k)^2}\frac{a}{2}\right]-\phi_{++}^{\mathrm{SR}}\left[\sqrt{i^2+j^2+k^2}a\right]\right\}.$$

Similarly, the anion–anion short-range interactions $E_{--}^{\mathrm{B1-SR}}(a)$ and $E_{--}^{\mathrm{B2-SR}}(a)$ are the sums of pair potential $\phi_{--}^{\mathrm{SR}}(r)$ for B1- and B2-KCl, and the cation–anion short-range interaction $E_{+-}^{\mathrm{B2-SR}}(a)$ can also be obtained; then, the cation–cation short-range pair potential $\phi_{++}^{\mathrm{SR}}(r)$ can also be obtained by Chen–Möbius lattice inversion [15,16].

After the interionic pair potential curves of KCl have been derived from total energies of the above four KCl crystals, in terms of the shapes of short-range pair potential curves, the Morse function is selected to well fit the anion–anion short-range pair potential, and exponential repulsive functions to perfectly fit the cation–anion short-range pair potentials, the short-range cation–cation interaction being so small that it can be neglected. Then, the final interionic pair potentials can be written as

$$\Phi_{+-}(r) = \phi_{+-}^{\mathrm{SR}}(r) + \phi_{+-}^{\mathrm{Coul}}(r) \tag{11}$$
$$= D_{+-}\exp\left[\gamma_{+-}\left(1-\frac{r}{R_{+-}}\right)\right] + \frac{q_+q_-}{4\pi\varepsilon_0 r},$$

$$\Phi_{--}(r) = D_{--}\left(\left[1-\exp\left(\gamma_{--}\left(1-\frac{r}{R_{--}}\right)\right)\right]^2 - 1\right) + \frac{q_-q_-}{4\pi\varepsilon_0 r}, \tag{12}$$

$$\Phi_{++}(r) = \frac{q_+q_+}{4\pi\varepsilon_0 r}, \tag{13}$$

and the potential parameters are listed in Table 1.

3. Static properties of B1 and B2 KCl

In order to test the quality of the present potentials, we first calculated the static properties of B1 and B2 KCl, e.g. equilibrium lattice constant a_0, bulk modulus B_0, lattice energy E_{latt} and volume V_0 at zero pressure. The results are listed in Table 2, and compared with the experimental data [25] and Zhang's calculations [23]. They are in good agreement.

With the inversion potentials, we can calculate the 0-K Gibbs free energy $G = E_{\mathrm{latt}} + PV + TS$ ($T = 0$ K), which equals the enthalpy H in the static limit. Then, the variation of G with P for both B1 and B2 phases is calculated as $G_{\mathrm{B1}} = -169.10 + 8.06P$ and $G_{\mathrm{B2}} = -167.02 + 7.26P$, with P in GPa and G in kcal/mol. The B1⟶B2 transition pressure P_{tr} is obtained by

$$G_{\mathrm{B1}}(P_{\mathrm{tr}},V_{\mathrm{B1}}) = G_{\mathrm{B2}}(P_{\mathrm{tr}},V_{\mathrm{B2}}) \tag{14}$$

The results are listed in Table 3, in which the experimental data [27] and the calculations of Recio et al. [26] and Zhang and Bukowinski [23] are also listed for comparison. The present calculated P_{tr} values are a little higher than the experimental data. In spite of the difference between our calculations and experimental data, overall agreement is obtained. This indicates that the present potentials can be used to further simulate the B1–B2 phase transition of KCl.

4. Transition path from B1 to B2 phase

According to the analyses of Pendás et al. [12] and Sims et al. [13], the B1 ($Fm\bar{3}m$ (2 2 5))–B2

Table 1
Interionic potential parameters derived by lattice inversion in this work. The short-range terms are truncated at a value of r_c = 10.00 Å

K–Cl			Cl–Cl			Effective charge	
D_{+-} (eV)	R_{+-} (Å)	γ_{+-}	D_{--} (eV)	R_{--} (Å)	γ_{--}	q_+	q_-
1.6286	2.3677	6.4711	0.1177	3.7066	8.8093	1.00e	−1.00e

Table 2
Calculated static properties of B1 and B2 KCl

Structure		Lattice constant a_0 (Å)	Bulk modulus B_0 (GPa)	Lattice energy E_{latt} (eV)	Volume at 0 Pa V_0 (Å^3)
B1	Present work	6.266	19.12	7.35	61.51
	Ref. [23]	6.200	19.35	7.40	62.04
	Ref. [25]	6.32	18.6	7.26	63.11
	Ref. [12]	6.524	15.5	7.07	69.14
	Expt. [25]	6.294	19.7	7.35	62.33
B2	Present work	3.794	23.15	7.25	54.61
	Ref. [23]	3.717	26.86	7.30	52.93
	Ref. [25]	3.76		7.13	
	Ref. [12]	3.385	19.6	6.96	
	Expt. [25]		31.6		51.87

Table 3
B1–B2 phase transition data, including pressure P_{tr}, bulk modulus B_t, volume V_t and their changes

	P_{tr} (GPa)	V_t (B1) (Å^3)	V_t (B2) (Å^3)	$\frac{-\Delta V_t}{V_t(B1)}$	B_t (B1) (GPa)	B_t (B2) (GPa)	$\frac{-\Delta B_t}{B_t(B1)}$
Present work	2.58	55.37	49.92	0.10	28.90	33.28	0.12
Ref. [26]	2	62.91	54.78	0.13	24	27	0.13
Ref. [23]	2.1			0.12			
Expt. [27]	2	57.01	50.33	0.122	–	–	–

($Pm\bar{3}m$ (2 2 1)) phase transition could be considered to take place along the Buerger $R\bar{3}m$ pathway for a two-ion unit cell. This way, lattice translational symmetry is assumed to hold throughout the transformation, which is modelled as a cooperative movement of atoms in an ideal crystal, neglecting the breaking of translational symmetry. However, it is true that there is both experimental and theoretical evidence indicating a very important role of defects in the kinetics of the transition [6,10]. Then the breaking of translational symmetry will be observed during the phase transition. In order to obtain more structural information about intermediate states along the transition path, fewer symmetric restrictions should be taken into account as far as possible. Therefore, based on the above inversion pair potentials, the intermediate structures were obtained within fewer symmetry restrictions than those of the $R\bar{3}m$ space group. The details are described as follows.

For the two-ion rhombohedral cell in Fig. 3(a), if we assume Path I as the transition path including a series of $R\bar{3}m$ cells (a, a, a, α, α, α), with one inner atom ($x = y = z = 0.5$) at a given external pressure P, then the 0-K Gibbs free energy surface vs. cell angle α and length a could be calculated from interionic pair potentials. That is to say, each of the intermediate structures was obtained by relaxing the initial cell (a_0, a_0, a_0, α, α, α) to the minimum-energy state (a, a, a, α, α, α) for each fixed angle α.

Path I

$$\underset{Fm\bar{3}m}{\left(a_0,a_0,a_0,\frac{\pi}{3},\frac{\pi}{3},\frac{\pi}{3}\right)}\longrightarrow\underset{\frac{\pi}{3}\le\alpha\le\frac{\pi}{2}}{(a,a,a,\alpha,\alpha,\alpha)}\longrightarrow\underset{Pm\bar{3}m}{\left(b_0,b_0,b_0,\frac{\pi}{2},\frac{\pi}{2},\frac{\pi}{2}\right)}.$$

This path in Fig. 4(a) shows that B1 and B2 are two local minima at zero pressure, and that B1 is lower than B2. With the increase of pressure P, the B1 and B2 states undergo the reverse changes, the

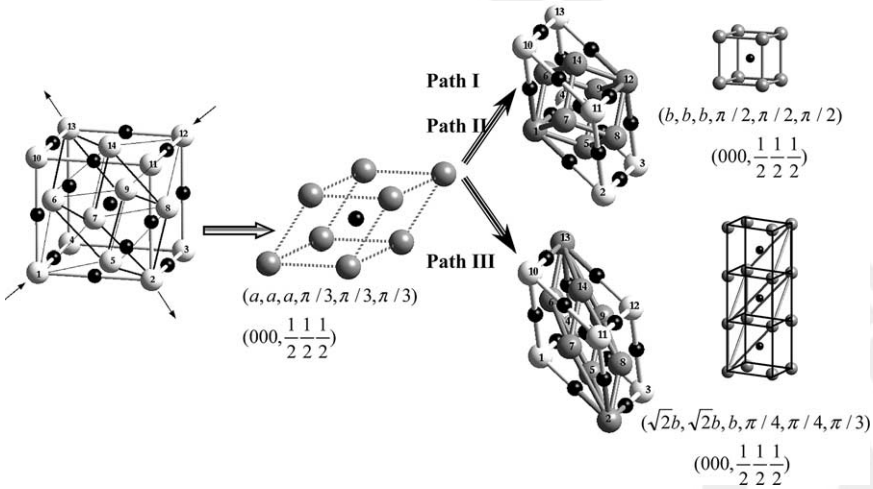

Fig. 3. Transition path in two-ion cell for conversion of B1 into B2 phase. One B1 and two equivalent B2 primitive cells are shown by dark grey balls. Path I ($R\bar{3}m$ path) and Path II are from rhombohedral (a) to simple cubic (b), and Path III connecting (a) and (c) rhombohedral cells.

first one rising from the minimum to the saddle point, and the second changing from a minimum to a deeper one. The coupling of the a, α coordinates along the path as a function of pressure P is shown in Fig. 4(b). The parallel curves indicate that pressure P cannot change the a, α coupling for the constrained symmetry. This is the $R\bar{3}m$ path connecting the B1 and B2 phases, which is in agreement with Pendás et al. [12].

The above transition path is obtained within the restriction of space group $R\bar{3}m$, i.e. the cell length a is optimized with regard to a fixed angle α. If the translational symmetry can be broken to determine the intermediate structures, the transition path may be described as Path II (a, b, c, α, β, γ).

Path II

$$\left(a_0,a_0,a_0,\underset{Fm\bar{3}m}{\tfrac{\pi}{3},\tfrac{\pi}{3},\tfrac{\pi}{3}}\right)\rightarrow(a,b,c,\alpha,\beta,\gamma)\rightarrow\left(b_0,b_0,b_0,\underset{Pm\bar{3}m}{\tfrac{\pi}{2},\tfrac{\pi}{2},\tfrac{\pi}{2}}\right).$$

Different from the $R\bar{3}m$ path, from the same initial cell (a_0, a_0, a_0, α, α, α) to the minimum-energy state, the cell parameters a, b, c, β, γ and inner atomic position (x, y, z) are independently optimized to make the energy minimum for each fixed angle α from $\pi/3$ to $\pi/2$. Then the transition path can be described by Fig. 5(a) at transition pressure P_{tr}. With fewer symmetric restrictions, the relationships $a = b = c$, $\alpha = \beta = \gamma$ and $x = y = z = 0.5$ cannot be kept unchanged for all intermediate structures; then, Path II could be divided into three parts, corresponding to space groups $R\bar{3}m$, $C2/m$ (12) and $Cmmm$ (65), respectively. This indicates that the transition path may not always be on the $R\bar{3}m$ surface, and will include a series of states with some common subgroups between $Fm\bar{3}m$ and $Pm\bar{3}m$ symmetries. In Fig. 5(b), the cell parameters as a function of α show that Path II is very close to Path I near the B1 state, but is obviously different from Path I near the B2 phase. By comparing the energy of Path I with that of Path II, it is obvious that the Gibbs energy of each state of Path II is less than or equal to that of Path I. This may be the reason that Path II is a more reasonable trace from B1 to B2, in spite of the identical activation energy for both Paths I and II.

It is worth noting that the variation of restrictions will also lead to different paths. Then Path III is introduced in terms of the final relaxed configuration at 30 GPa, as shown in Fig. 3(c). Since the energy minimization path may not be so convincing as the transition path, Path III was determined as follows.

Path III

$$\left(a_0,a_0,a_0,\underset{Fm\bar{3}m}{\tfrac{\pi}{3},\tfrac{\pi}{3},\tfrac{\pi}{3}}\right)\rightarrow\left(a,b,c,\alpha,\beta,\underset{\frac{\pi}{3}\geq\alpha\geq\frac{\pi}{4}}{\tfrac{\pi}{3}}\right)\rightarrow\left(\sqrt{2}b_0,\sqrt{2}b_0,b_0,\underset{Pm\bar{3}m}{\tfrac{\pi}{4},\tfrac{\pi}{4},\tfrac{\pi}{4}}\right).$$

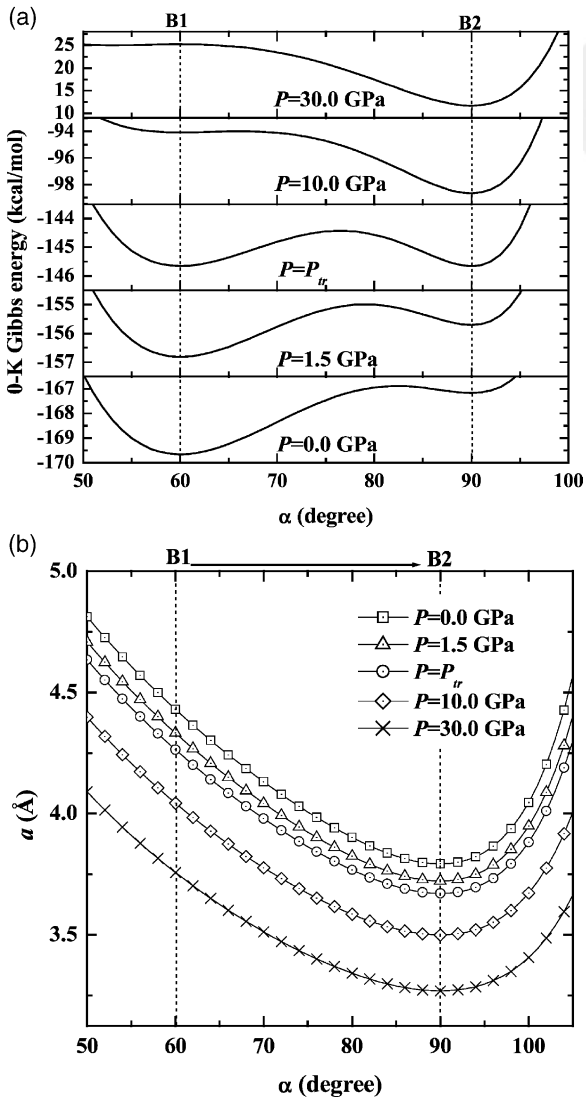

Fig. 4. The 0-K Gibbs energy as a function of pressure P and rhombohedral angle α (a), and the corresponding a–α coupling along Path I (b).

Now Path III is assumed as (a, b, c, α, β, $\pi/3$), where angle α decreases from $\pi/3$ to $\pi/4$. For each fixed angle α, the cell parameters a, b, c, β and inner atomic position (x, y, z) were independently adjusted to make the cell energy minimum. The restrictions are different from that of Path II. The predicted cell parameters of intermediate structures are presented as shown in Fig. 5(c). Due to the fewer symmetric restrictions, Path III is also a mul-

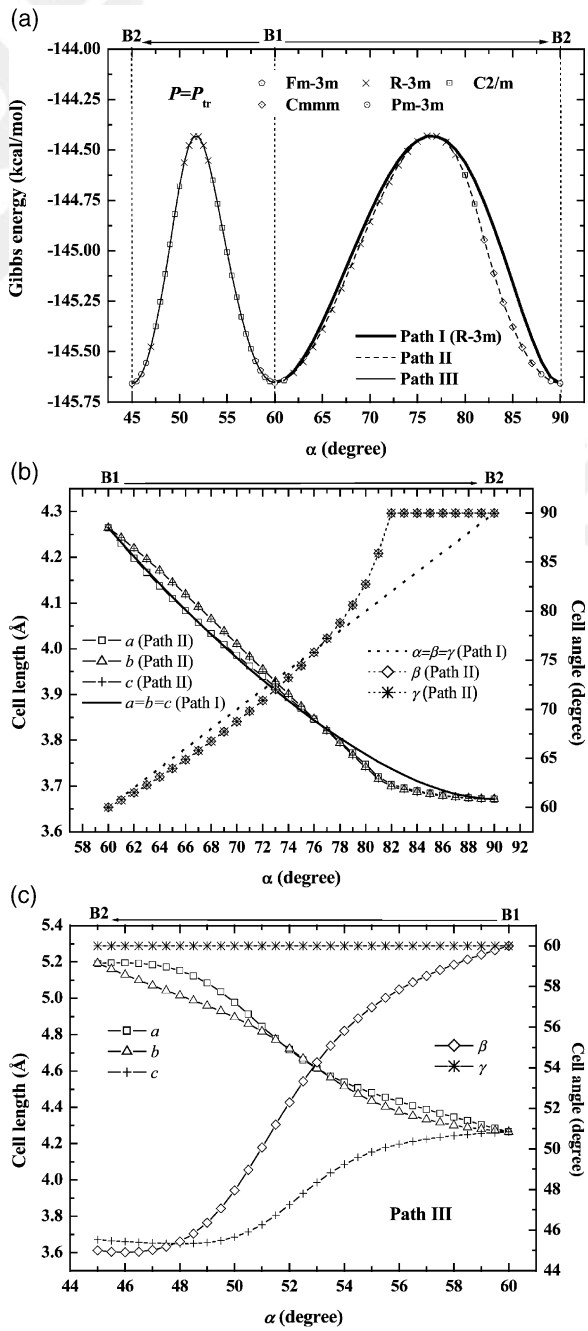

Fig. 5. (a) 0-K Gibbs energies as a function of cell angle α of Paths I, II and III, marked by thick, dashed and thin lines at transition pressure P_{tr}, respectively. (b) The cell parameters as a function of cell angle α along Path II, compared with those of Path I. (c) The cell parameters as a function of cell angle α along Path II.

tiple-symmetry pathway connecting B1 and B2 states, including $C2/m$ and $R\bar{3}m$ states. Since the constrained condition of $\gamma = \pi/3$ is not applied, Path II has three kinds of intermediate states, more than those of Path III. The barrier between B1 and B2 phases indicates that the activation energy of Path III is equal to that of Paths I and II (see Fig. 5(a)). Then from this viewpoint, it may be inferred that Paths I, II and III are essentially equivalent for B1 to B2 phase transition.

Although Paths I, II and III have been obtained for describing the B1–B2 phase transition in the two-ion KCl cell, the transition path may also depend on the size of unit cell besides the symmetry. Sims et al. [13] reported the $Pmm2$ path in a four-ion cell for describing the WTM mechanism, which involved four independent variables. Since we do not want to repeat the $Pmm2$ path as that of Sims, we use a eight-ion standard cell to present Path IV for the B1–B2 phase transition here. Similarly, based on the relaxation from B1 to B2 structure at 30 GPa (see Fig. 6), Path IV is defined as:

Path IV

$$\underset{Fm\bar{3}m}{\left(a_0,a_0,a_0,\frac{\pi}{3},\frac{\pi}{3},\frac{\pi}{3}\right)} \rightarrow \underset{90°\geq\alpha\geq 70.53°}{(a,b,c,\alpha,\beta,\beta)} \rightarrow \underset{Pm\bar{3}m}{(b_0,b_0,b_0,109.47°,70.53°,70.53°)}.$$

The intermediate structure along the transition path is described as the cell (a, b, c, α, β, β) with optimized inner atomic positions. For each point along the transition path, the structural parameters were then calculated by optimizing the cell parameters a, b, c, α and inner atomic positions to the minimum energy, with regard to a fixed β from 90° to 70.53°. The number of independent variables obviously increased. The results are shown in Fig. 7, and the corresponding Gibbs energy as a function of cell angle β ($\beta = \gamma$) indicates that the phase transition takes place along the $C2/m$ path at the first stage, followed by a short $R\bar{3}m$ path to the saddle point, then transforming to the $P2_1/m$ (11) states, and stepping towards the B2 phase along the $C2/m$ path. During the $P2_1/m$ part, the $CmCm$ (63) structure occurs, and the $P1$ (2) state appears to connect the $P2_1/m$ and $C2/m$ parts. This result also indicates that the symmetry of transition of the transition path is not always kept unchanged, and the B1 and B2 states are connected by different parts with different subgroup symmetries.

5. Discussion and conclusions

Based on the present potentials, four transition pathways were proposed to describe the B1–B2 transformation in KCl. Although their saddle points have the same space group $R\bar{3}m$ and the heights of barriers change only a little, the results in Figs. 5(a) and 7(a) indicate that if one allows more breaking of symmetry along the path, an intermediate phase with a smaller subgroup than $R\bar{3}m$ will occur and lead to a slightly lower energy path, Path IV, whose barrier is ~0.15 kcal/mol smaller than that of the two-ion cell.

Especially for Path IV, the number of independent variables is obviously more; some new intermediate structures can be determined on an

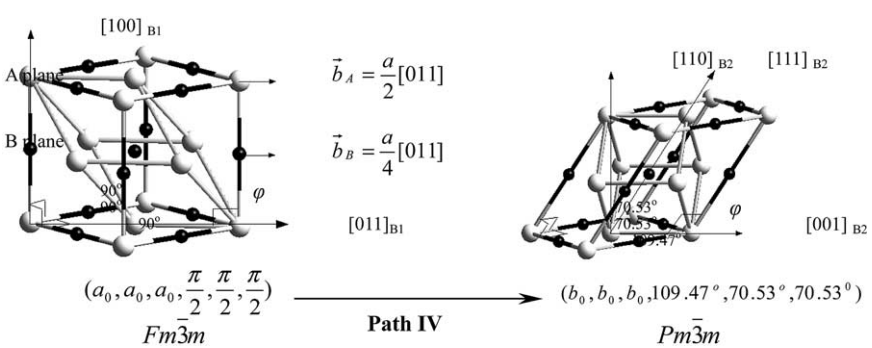

Fig. 6. The initial and final configurations of the eight-ion standard cell along Path IV, in which the reorientation and relation, displacement of (0 0 1) planes along [0 1 1] direction and the angle ϕ between [1 0 0] and [0 1 1] directions are separately indicated.

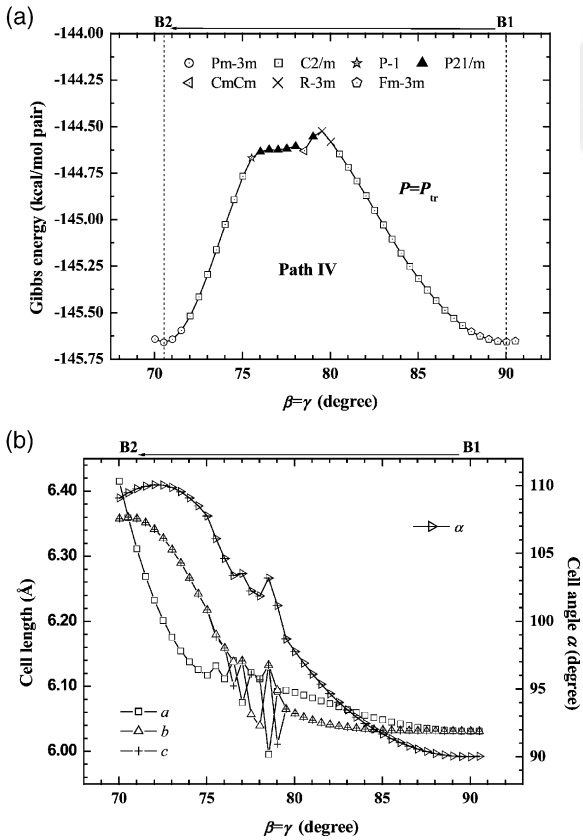

Fig. 7. (a) 0-K Gibbs energy as a function of cell angle β ($\beta = \gamma$) along Path IV at P_{tr}. (b) Cell parameters vs. cell angle β ($\beta = \gamma$) along Path IV at P_{tr}.

energy hypersurface with more dimensions, such as the $P2_1/m$ and $P\bar{1}$ structures. Due to the appearance of $P\bar{1}$ structure, the translational symmetry of the cell is drastically lowered. The structure with the $P\bar{1}$ space group could be considered evidence of the breaking of translational symmetry. In the meantime, the intermediate structure with the $P2_1/m$ space group is also surprising, because by in situ X-ray diffraction, both Kusaba et al. [28] and Hull and Keen [29] reported the KOH-type intermediate structure with space group $P2_1/m$ in the B1–B2 phase transition of AgCl, in which the angle ϕ between [1 1 0] and [0 0 1] directions of B1 structure is 101°, which exactly corresponds to the point of Fig. 7(b) when the angle β is 77.03°, and the corresponding angle ϕ 101.7°. Although the $P2_1/m$ structure has not been found in the KCl experiments, it is possible that there are common B1–B2 phase transition characters for both ACl and KCl crystals.

The two-ion or four-ion cell can only present one-side transition characters, but characters of both Buerger and WTM mechanisms can be described in the eight-ion standard cell. As shown in Fig. 6, the rhombohedral cell is compressed along the threefold axis into the simple cubic cell, corresponding to Buerger transition. With regard to the WTM mechanism, the A plane glides with Buerger vector $\vec{b}_A = (a/2)[0\,1\,1]$, and $\vec{b}_B = (a/4)[0\,1\,1]$ for B plane, which leads to relative displacement $(a/4)[0\,1\,1]$ between adjacent (1 0 0) planes, where a is the lattice parameter. Moreover, the orientation relation of [1 1 0](B2)//[1 $\bar{0}$ 0](B1), [1 0 $\bar{0}$](B2)//[0 1 1](B1) and [1 1 $\bar{1}$](B1)// [1 1 1](B2) has also been reflected in Fig. 6. This result is in good agreement with previous calculations [9,11] and experimental results [8]. Therefore, with fewer symmetry restrictions, the larger unit cell not only provides more details about the transition path, but also more characteristic features of phase transition than the two-ion cell with $R\bar{3}m$ symmetry.

Among the four pathways, Paths II, III, IV are obtained by optimizing more than eight independent variables. The number of independent variables is too many to be considered by ab initio methods. Even for the force-field method, interionic potentials are also required to be valid over a wide range of interionic separations and coordination environments. Otherwise, a reasonable pathway cannot be obtained. Therefore, the interionic potentials play an important role, and their quality determines whether or not the phase transition from B1 to B2 phase can be correctly described. Based on the present interionic pair potentials, the calculated static properties of B1- and B2-KCl are in good agreement with the experimental results and previous calculations. Using the two-ion and eight-ion cells, we have proposed four minimum-energy transition pathways with different symmetric restrictions. Path I is quite consistent with the previous $R\bar{3}m$ path, but the other three transition pathways are distinct from the previous Buerger and WTM pathways, which provide more detail about the phase transition. The predicted

intermediate structures may be found in further experiments. This fully proves that it is reasonable that the B1–B2 phase transition in KCl should be considered by using the larger size unit cell with fewer symmetric restrictions with the appropriate interionic potentials, such as the inversion pair potentials.

6. Uncited reference

[24].

Acknowledgements

This work was supported in part by the National Nature Science Foundation of China (Grant No. 10274035), and in part by the National Advanced Materials Committee of China. Special thanks go to the support from the 973 Project in China (No. G2000067101).

References

[1] Al'tshuler LV, Pavlovskii MN, Kuleshova LV, Simakov GV. Sov Phys-Solid State 1963;5:203.
[2] Hayes DB. J Appl Phys 1974;45:1028.
[3] Duvall GE, Graham RA. Rev Mod Phys 1977;49:523.
[4] Rosenberg Z. J Appl Phys 1982;53:1474.
[5] Zaretsky EB, Kanel GI, Mogilevsky PA, Fortov VE. Sov Phys Dokl 1991;36:76.
[6] Zaretsky EB. J Phys Chem Solids 1998;59:253.
[7] West AR. Solid state chemistry and its applications. New York: Wiley, 1984.
[8] Watanabe M, Tokonami M, Morimoto N. Acta Cryst 1977;A33:294.
[9] Nakagiri N, Nomura M. J Phys Soc Jpn 1982;51:2412.
[10] Ruff I, Baranyai A, Spohr E, Heinzinger K. J Chem Phys 1989;91:3148.
[11] Nga YA, Ong CK. Phys Rev B 1992;46:10547.
[12] Pendás AM, Luaña V, Recio JM, Flórez M, Francisco E, Blanco MA, Kantorovich LN. Phys Rev B 1994;49:3066.
[13] Sims CE, Barrera GD, Allan NL. Phys Rev B 1998;57:11164.
[14] Allan NL, Barrera GD, Purton J, Sims CE, Taylor MB. Phys Chem Chem Phys 2000;2:1099.
[15] Chen N-X, Chen Z-D, Wei Y-C. Phys Rev E 1997;55:R5.
[16] Chen N-X, Ge X-J, Zhang W-Q, Zhu F-W. Phys Rev B 1998;57:14203.
[17] CASTEP, Molecular Simulation Software, 1998.
[18] Yoji I, Masakazu M, Tatsuo T. Thin Solid Films 2001;381:176.
[19] Segall MD, Lindan PJ, Prober MJ, Pickard CJ, Hasnip PJ, Clark SJ et al. J Phys: Condens Matter 2002;14:2717.
[20] Monkhorst HJ, Pack JD. Phys Rev B 1976;13:5188.
[21] Kittel C. In: Introduction to solid state physics. 7th ed. New York: John Wiley & Sons, Inc; 1996. p. 66–72.
[22] Ewald PP. Ann Phys 1921;64:253.
[23] Zhang H, Bukowinski MST. Phys Rev B 1991;44:2495.
[24] Francisco E, Recio JM, Blanco MA, Pendás AM, Pueyo L. Phys Rev B 1995;51:2703.
[25] Cohen AJ, Gorden RG. Phys Rev B 1975;12:3228.
[26] Recio JM, Pendás AM, Francisco E, Flórez M, Luaña V. Phys Rev B 1993;48:5891.
[27] Vaidya SN, Kennedy GC. J Phys Chem Solids 1971;32:951.
[28] Kusaba K, Syono Y, Kikegawa T, Shimomura O. J Phys Chem Solids 1995;56:751.
[29] Hull S, Keen DA. Phys Rev B 1999;59:750.